Optimal Sensor Mobility Design for Target Tracking with Distributed Sensing, Communication and Computing Infrastructure

Vahram Stepanyan *
NASA Ames Research Center, KBR Wyle Services, Moffett Field, CA 94035

Corey Ippolito †
NASA Ames Research Center, Moffett Field, CA 94035

Evan T. Kawamura‡
NASA Ames Research Center, Moffett Field, CA 94035

Thomas Lombaerts§
NASA Ames Research Center, KBR Wyle Services, Moffett Field, CA 94035

The paper presents an airborne target tracking approach with data fusion from distributed stationary and mobile sensor network transmitted through a wireless/wired communication network and using a distributed computing infrastructure. To obtain high quality measurements, sensor flight platforms' positions and orientations are optimized with respect to the available target's position and velocity estimates, and a formation control strategy is applied to derive desired trajectories for the flight platforms. As sensors move, the communication network topology switching is determined using the worst-case approach to handle uncertainties in the target's and sensors' positions, which alters communication delays for sensors' data transmission to computing centers. An optimal data migration algorithm is periodically applied to determine these communication delays for each sensor and the optimal location with minimum end-to-end latency for the target tracking algorithm execution, which is based on adaptive information fusion from multi-modal mobile and stationary sensors inside an Extended Kalman Filter framework. The approach is validated in a desktop simulation environment using synthetic sensor data generated for a simulated target's flight.

I. Introduction

Advancing airborne autonomy is essential to Advanced Air Mobility operations for autonomous passengers and cargo delivery in dense and highly dynamic metropolitan areas, which can be strengthened by distributed sensing and cooperative reasoning. This technology is capable of supporting functions such as detect-and-avoid, monitoring and surveillance of the airspace along urban corridors using both ground based and airborne observations, communications and computing infrastructure that is distributed across the airspace to meet the emerging needs of advanced urban operations in the national airspace [1]. Primary distributed sensing and cooperative reasoning research efforts for abstraction of the problem, identification of requirements and constraints for operations, and algorithmic constructs addressing challenges in developing a dynamic, topologically-adaptive, and accurate estimation system are presented in Ref. [2].

Independent surveillance of the airspace through a distributed ground sensing network is a key technology for extraction of accurate and in-time information about airspace to provide situational awareness and make informed decisions for safe operations in the presence on both cooperating and-non-cooperating air vehicles. One of the highly researched area of surveillance is target tracking, which traditionally was conducted using ground based radars (See for example [3–10] and references therein). However, radar's range and angle measurements may have different

*Technical Advisor, KBR Wyle Services, Intelligent Systems Division, Mail Stop 269-1, email: vahram.stepanyan@nasa.gov
†Aerospace Research Engineer, Intelligent Systems Division, Mail Stop 269-1, email: corey.a.ippolito@nasa.gov
‡Aerospace Research Engineer, Intelligent Systems Division, email: evan.t.kawamura@nasa.gov
§Aerospace Research Engineer, KBR Wyle Services, Intelligent Systems Division, Mail Stop 269-1, email: thomas.lombaerts@nasa.gov

accuracy depending on the configurations [3]. In majority of cases, the target motion is considered as a continuous time coordinate-uncoupled white-noise linear model for a point object [5, 6] with nonlinear measurements, and the tracking is done in the Extended Kalman Filter (EKF) framework.

More accurate results are obtained combining radar measurements with visual ones [11–14]. Ref. [11] fuses radar and vision measurements to compare several Extended Kalman Filter (EKF) based trackers, Ref. [12] presents an object tracking algorithm based on the EKF that uses distributed ground-based sensors with specific properties and limitations, Ref. [13] addresses a tracking problem for a non-cooperating airborne target using an adaptive information fusion from a ground based distributed sensors with communication delays, Ref. [14] considers air vehicles classification problems using velocity-based metrics.

As target moves through the airspace, ground based sensors will have temporary opportunistic observations of the it. One way to improve the data acquisition is to have a fleet of aircraft carrying a heterogeneous set of sensors in addition to ground based sensor network. Since various sensors have various sensing range and angles for the best perception of the target, the challenge here is to determine an optimal formation for these sensor platforms, and design navigation strategies to track the formation without collision. To this end, any available in the literature formation flight approaches can be used (see for example [15–20] and references therein).

Other challenge for mobile sensors based collective reasoning involves uncertainty in the topological structure of the estimation problem, with uncertainty and variability both temporally and spatially in the topology of data transmission network. Therefore, to make an in-time decision for safe and reliable airspace operations, it is necessary to automatically determine where to execute the reasoning algorithm while satisfying the quality of service constraints. Ref. [23] presents an approach to data and reasoning optimal migration utilizing edge computing infrastructure to meet system's latency, cost and power consumption requirements given the communication network and computing hardware limitations.

In this paper we integrate several technologies to design optimal trajectories for mobile sensors, to adaptively fuse information from both stationary and mobile sensors received over a wired/wireless communication network by the selected computing center with minimum end-to-end latency, and to track a non-cooperating aircraft using the EKF framework that takes into account information delays. To obtain high quality measurements, sensor flight platforms' positions and orientations are optimized with respect to available target's position and velocity estimates, and a formation control strategy is applied to derive desired trajectories for the sensor carrying air vehicles. As sensors move, the communication network topology switching is determined using the worst-case approach to handle uncertainties in the target's and sensors' positions, which alters communication delays for sensors' data transmission to computing centers. An optimal data migration algorithm is periodically applied to determine these communication delays for each sensor and the optimal location with minimum end-to-end latency for the target tracking algorithm execution, which is based on adaptive information fusion from multi-modal mobile and stationary sensors inside an Extended Kalman Filter framework.

II. Problem Formulation

We consider a set of n_s heterogeneous sensors s_i, $i = 1,\dots,n_s$, both stationary and mobile, which are distributed across a region of interest. We assume that positions of the sensors $\boldsymbol{p}_i^s$, $i = 1,\dots,n_s$ in a Cartesian ENU (East-North-Up) frame F_0 is known at each time instance. They provide multi-modal multi-rate information about the associated airspace through an available wired and/or wireless communication network to a monitoring observer. It is assumed that the stationary sensors have fixed orientation with respect to F_0, which are given by rotation matrices $\mathbb{R}_i$, $i = 1,\dots,n_s$ from sensor specific frames F_i^s, $i = 1,\dots,n_s$ to F_0, whereas the mobile sensors are mounted on air vehicles capable of automatically follow the observer's commands, with their best viewing directions aligned with vehicles longitudinal axis. We assume that independent of the produced by sensors data type and size, the packages to be transmitted over the communication network also include time information when the data were recorded and processed by associated with the sensors computing units.

Let the transmitting towers t_i, $i = 1,\dots,N_t$ be located at $\boldsymbol{p}_i^t$, $i = 1,\dots,n_t$ in the frame F_0 and have maximum transmit power of w_i^t, $i = 1,\dots,n_t$ (in watts) for wireless transmission. Based on these powers and the adopted communication model, a maximum transmit distance $d_i^{\max}$, $i = 1,\dots,n_t$ for each tower can be computed from the perspective of an acceptable signal to noise ratio. Additionally, we assume that the sensors have transmission power of w_i^s, $i = 1,\dots,n_s$, which is sufficient to reach the closest tower. All wired connection legs have a uniform rate of ω (in bits per second). Both stationary and mobile sensors transmit the recorded data through the closest tower no matter a wired or wireless communication is used. This implies that each sensor communicates with only one tower at a time based on the separation distance from it and switches to the next tower as it crosses the coverage area borderline.

We will denote $s_i \in H(t_k)$ to indicate that the sensor s_i is in the coverage area $H(t_k)$ of tower t_k. As mobile sensors move through the environment, the communication topology changes, which results in variable transmission delays for the corresponding information to reach the observer and data processing center. This necessitates finding of an optimal location for the data processing with a minimum end-to-end latency periodically as the sensors move in the same coverage area and each time the communication topology switches are predicted.

We assume that the monitoring observer has access to a network of edge/cloud computing centers c_i, $i = 1,\dots,n_c$ with known computing capabilities to be utilize for sensor data processing. Let the locations of this centers be $\boldsymbol{p}_i^c$ $i = 1,\dots,n_c$ in the frame F_0. We assume that the computing centers are stationary and wired connected to the closest communication towers.

The objective is to provide continuous and persistent estimates of the state of a non-cooperating aircraft operating within the airspace to a monitoring observer with the minimum end-to-end latency. We notice that this latency also includes the elapsed time for all algorithms execution. Therefore, for the purpose of this paper, we will focus on fast algorithms, which may end-up being only sub-optimal.

III. Optimal Sensor Navigation

In this section we formulate problems of finding the sensors' positions for optimal and robust data acquisition and defining the trajectories to track these optimal positions at each time instance given the best available estimate of the target aircraft's position. Let this position be $\boldsymbol{p}_a$ in the frame F_0, and there be n_s^m mobile sensors s_i^m, $i = 1,\dots,n_s^m$ taking measurements of $\boldsymbol{p}_a$. Each sensor has its own optimal measurement distance from the target given as a range of $\rho_i^{\min} \le d_{ia} \le \rho_i^{\max}$, where $d_{ia} = d(s_i^m, a) = \|\boldsymbol{p}_i^s - \boldsymbol{p}_a\|$, and minimum safe separation distance ρ_{ij} form other sensors for each $i, j = 1,\dots,N_s^m$, $i \neq j$. Here, $\rho_i^{\min}$ is chosen to also provide a safe separation from the target. Let the angle between direction vectors $\boldsymbol{e}_j$ and $\boldsymbol{e}_{ja}$, which is called line-of-sight (LOS) angle here, be φ_j, where $\boldsymbol{e}_j$ indicates the $j-th$ sensor's direction of flight and $\boldsymbol{e}_{ja}$ indicates the $j-th$ sensor to the target's estimated position $\boldsymbol{p}_a$ direction. Fig. 1a displays LOS angles for a two sensors carrying air vehicles scenario.

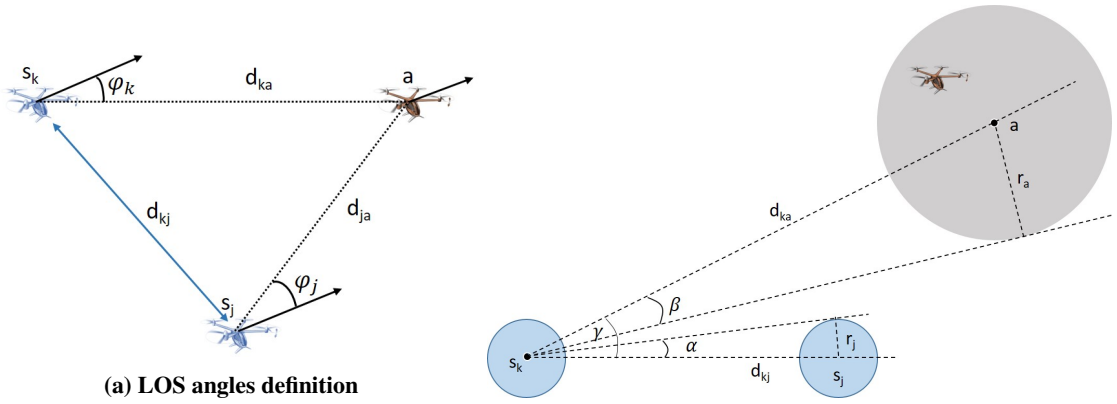

(a) LOS angles definition

(b) Occlusion prevention angles definition

Fig. 1 Two mobile sensors scenario.

Let the error in target aircraft's position estimation be of size r_a, that is the target aircraft can be at any point inside a ball of radius r_a centered at $\boldsymbol{p}_a$, which is displayed in Fig. 1b as a gray circle. In order to take into account the sizes of sensor carrying air vehicles into the navigation algorithm, we represent them as balls of radius r_j centered at $\boldsymbol{p}_j^s$ for each $j = 1,\dots,N_s^m$, which are displayed in Fig. 1b as blue circles. Then the occlusion prevention can be enforced by the condition $\alpha_{kj} + \beta_k \le \gamma_k$, where $\alpha_{kj} = \arcsin\left(r_j/d_{kj}\right)$, $\beta_k = \arcsin\left(r_a/d_{ka}\right)$, and $\gamma_k = \arccos\left(\boldsymbol{e}_{ka}^\top \boldsymbol{e}_{kj}\right)$, and $\boldsymbol{e}_{kj}$ indicates the direction from sensor s_k^m to sensor s_j^m.

The best data acquisition for the $i-th$ sensor takes place when φ_i is as small as possible given the measurement distance and safe separation constraints assuming that no sensor is occluded. Therefore, the optimal sensors placement

can be obtained by solving the following optimization problem

$$\begin{aligned} \min_{\phi_i,\ i=1,\ldots,N_s^m} \quad & \sum_{i=1}^{n_s^m} c_i^s \phi_i^2 \\ \text{subject to:} \quad & \rho_i^{\min} \le d(s_i^m, a) \le \rho_i^{\max},\ i = 1,\ldots,n_s^m \\ & \rho_{ij} \le d(s_i^m, s_j^m) \\ & \alpha_{ij} + \beta_i \le \gamma_i,\ i,j = 1,\ldots,n_s^m,\ i \ne j \end{aligned} \tag{1}$$

The sensors optimal position $\boldsymbol{p}_i^0$ make a desired formation for sensor carrying air vehicles to follow the target. Any state of the arts formation control method can be applied to maintain the optimal sensor placement for data acquisition. Here, we follow the steps of Ref. [15, 16, 19] and design formation tracking acceleration controls with collision avoidance for the sensors kinematic models

$$\begin{aligned} \boldsymbol{p}_i^s &= \boldsymbol{v}_i^s \\ \boldsymbol{v}_i^s &= \boldsymbol{u}_i,\ i = 1,\ldots,n_s^m \end{aligned} \tag{2}$$

as $\boldsymbol{u}_i = \boldsymbol{u}_i^t + \boldsymbol{u}_i^r + \boldsymbol{u}_i^a$, where $\boldsymbol{u}_i^t$ is the formation tracking part, $\boldsymbol{u}_i^r$ is the reference following part and $\boldsymbol{u}_i^a$ is the avoidance part. We notice that using kinematic models instead of full dynamics is not overly restrictive taking into account that the full dynamics can be reduced to a kinematic model by means of a feedback linearization (see for example [16]). The tracking control for each mobile sensor $i = 1,\ldots,n_s^m$ is designed as $\boldsymbol{u}_i^t = -k_1\left(\boldsymbol{p}_i^s - \boldsymbol{p}_i^0\right) - k_2\boldsymbol{v}_i^s$, where $k_1 > 0$ and $k_2 > 0$ are the properly chosen control gains, the reference control is designed as $\boldsymbol{u}_i^r = -c_1\left(\boldsymbol{p}_i^s - \boldsymbol{p}_r\right) - c_2\left(\boldsymbol{v}_i^s - \boldsymbol{v}_r\right)$, where $c_1 > 0$ and $c_2 > 0$ are the properly chosen control gains, $\boldsymbol{p}_r$ and $\boldsymbol{v}_r$ are respectively the reference position and velocity for the formation to follow, and the collision avoidance control is

$$\boldsymbol{u}_i^a = -\sum_{j=1, j\ne i}^{n_s^m+1} \frac{4(\rho_0^2 - \rho_{ij}^2)\left(d^2(s_i^m, s_j^m) - \rho_0^2\right)}{\left(d(s_i^m, s_j^m)2 - \rho_{ij}^2\right)^3}\left(\boldsymbol{p}_i^s - \boldsymbol{p}_j^s\right), \tag{3}$$

when $\rho_{ij} \le d_{ij} \le \rho_0$ and $\boldsymbol{u}_i^a = 0$ otherwise. Here we denote $\boldsymbol{p}_{n_s^m+1}^s = \boldsymbol{p}_a$, $\rho_{i,n_s^m+1} = \rho_i^{\min}$, and $\rho_0 = \max\{\rho_i^{\max},\ i = 1,\ldots,n_s^m\}$.

IV. Adaptive Communication Topology

In this section we provide a communication topology switching method from the perspective of optimizing the data transmission time from the flying sensors to computing centers. To this end, we assume a non-orthogonal multiple access (NOMA) wireless communication network with uniform hexagonal coverage areas, which allows all users to utilize the entire system bandwidth simultaneously with a multiple access interference in the coverage area, but neglect the interference between adjacent coverage cells [21, 22], and the towers communicate via a dedicated wired or wireless channels among themselves.

As the sensing aircraft crosses the boarder of an old cell, the communication automatically switches to the new tower. However, whether the aircraft will cross the boarder during a time interval of length τ_s associated with next round of data acquisition, processing and transmission depends on the direction of flight, which is not known a priory. We recall that in the ideal case, the mobile sensors fly in the leader following formation obtained in the previous section, hence have the same velocity $\boldsymbol{v}_a$ as the target aircraft. In reality though, these velocities will match with the accuracy of $\Delta\boldsymbol{v}_a$. That is the mobile sensors velocity can be expressed as $\boldsymbol{v}_s = \boldsymbol{v}_a + \Delta\boldsymbol{v}_a$. Hence there is an ambiguity in the communication topology associated with target aircraft's state estimation error, the corresponding bound of which can be obtained from the error covariance matrix that is computed at each estimation step in the EKF framework. Therefore, in the next data acquisition time instance the $i-th$ mobile sensor's position can be predicted at any point in a ball $B_i(r_i^s, \boldsymbol{p}_i^s)$ of radius $r_i^s = v_m\tau_s$ and centered at the sensor's current location $\boldsymbol{p}_i^s$, where $v_m = \|\boldsymbol{v}_a\| + \max\|\Delta\boldsymbol{v}_a\|$ and the maximum is taken over the EKF executed time steps in the duration of τ_s time interval preceding the current time. This ball constitutes a conservative estimate of the uncertainty region associated with the sensor's mobility and the target's state's estimation errors. The objective is to find the worst sensor position in $B_i(r_i^s, \boldsymbol{p}_i^s)$, which maximizes the communication time.

Let the data transmission time from sensor s_i^m to computing center c_k be $\tau(D(s_i^m),d(s_i^m,c_k)) = \tau(D(s_i^m),d(s_i^m,t_j))+ \tau(D(s_i^m),d(t_j,c_k))$ assuming the sensor communicates through the tower t_k. Here, $\tau(D(s_i^m),d(s_i^m,t_j))$ is the wireless data transmission time from s_i^m to t_j, which depends on the data size $D(s_i^m)$, sensor to tower distance $d(s_i^m,t_j)$ (the dependencies on the presence of other users in the coverage area and the network parameters are omitted for the convenience of notations), and $\tau(D(s_i^m),d(t_j,c_k))$ is the same data transmission time from t_j to c_k. Then, the worst case position $\boldsymbol{p}_i^0$ is found from the optimization problem

$$\max_{\boldsymbol{p}\in B(r_i^s,\boldsymbol{p}_i^s)} d(\boldsymbol{p},t_j)\,, \tag{4}$$

when $B(r_i^s,\boldsymbol{p}_i^s) \in H(t_j)$. Otherwise, when $B(r_i^s,\boldsymbol{p}_i^s)$ crosses the borderline of $H(t_j)$ into the adjacent coverage areas (at most two) $H(t_{j_i})$, $i = 1,2$, the worst case position is found from the following optimization problem

$$\max_{\boldsymbol{p}\in B(r_i^s,\boldsymbol{p}_i^s)} \max\left\{d(\boldsymbol{p},t_{j_i}),\ i = 0,1,2\|\right\} + \max\left\{\tau(D(s_i^m),d(t_{j_i},c_k)),\ i = 0,1,2\right\}\,, \tag{5}$$

where we denote $j_0 = j$. The resulting position $\boldsymbol{p}_i^0$ and index j_i^0 are used to estimate the end-to-end latency for the data from mobile sensor s_i^m to reach the computing center c_k via the communication tower $t_{j_i^0}$.

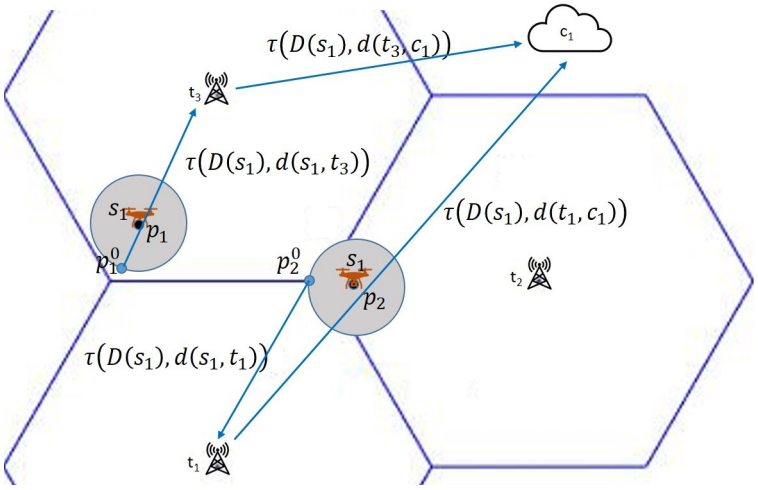

Fig. 2 Example of communication topology switch.

Fig. 2 displays an illustrative example of the communication topology adaptive switching based on the uncertainty region estimate, presented as gray circles. At the position p_1 the sensor s_1 transmits data to the computing center c_1 communicating through the tower t_3. There is no switching, and the algorithm (4) determines the worst case position $\boldsymbol{p}_1^0$ as the farthest point from the tower t_3, which is displayed as a blue dot in the figure, resulting in a prediction of the communication time $\tau(D(s_1),d(s_1,c_k)) = \tau(D(s_1),d(s_1,t_3)) + \tau(D(s_1),d(t_3,c_k))$. As the aircraft reaches position p_2, the sensor s_1 can communicate with any of three neighboring cells covering towers. Application of the algorithm (5) results in the optimal sensor position p_2^0 on the borderline of tower t_1 coverage area, which is depicted as a blue dot in the figure, and the sensor communicates with c_1 through tower t_1 with the elapsed time estimate prediction of $\tau(D(s_1),d(s_1,c_k)) = \tau(D(s_1),d(s_1,t_1)) + \tau(D(s_1),d(t_1,c_k))$.

V. Minimum latency Tracking

A. Optimal Computing Location.

Our goal is to find an optimal computing center to conduct target tracking with minimum end-to-end latency as the sensors move and a communication topology change is predicted. This latency includes time delays estimates for all available at the time sensor readings to reach the selected computing center and get processed through the Kalman filter algorithm. Here we follow the steps of Ref. [13] to compute the sensors readings transmission time delays and to

select the optimal computing location. The difference is that the data and service migration algorithm was executed in there just ones given the stationary infrastructure for sensing, networking and computing, but here it is executed each time sensors' positions noticeable change, which also takes into account the communication topology switching. The estimated delays are used in corresponding sensor measurement processing in EKF implementation.

B. Filter State Description.

We use a conventional continuous time coordinate-uncoupled white-noise acceleration model for a point object to describe the target's motion in Cartesian frame F_0 [5]

$$\begin{aligned} \ddot{x}(t) &= n_x(t) \\ \ddot{y}(t) &= n_y(t) \\ \ddot{z}(t) &= n_z(t)\,, \end{aligned} \tag{6}$$

where $n_x(t)$, $n_y(t)$, $n_z(t)$ are zero-mean, Gaussian distributed, and uncorrelated processes with variances σ_x^2, σ_y^2, σ_z^2. To apply EKF, we discretize the target dynamics with a time step δt. Then the filter's state evolution is described by the equations

$$\begin{aligned} \boldsymbol{s}(k|k-1)) &= \Phi(k-1)\boldsymbol{s}(k-1) \\ P(k|k-1) &= \Phi(k-1)P(k-1)\Phi^\top(k-1) + G\Gamma G^\top \\ \boldsymbol{s}(k) &= \boldsymbol{s}(k|k-1)) + W\left(\boldsymbol{h}(k) - \hat{\boldsymbol{h}}(k|k-1)\right)) \\ P(k) &= (\mathbb{I}_{7\times7} - W(k)M(k|k-1))P(k|k-1)(\mathbb{I}_{7\times7} - W(k)M(k|k-1))^\top + W(k)RW^\top(k)\,, \end{aligned} \tag{7}$$

where $\boldsymbol{s}(k) = [\hat{x}(k)\ \ \hat{y}(k)\ \ \hat{z}(k)\ \ \dot{\hat{x}}(k)\ \ \dot{\hat{y}}(k)\ \ \dot{\hat{z}}(k)\ \ \hat{b}(k)]^\top$, with $\hat{x}(k)$, $\hat{y}(k)$, $\hat{z}(k)$, $\dot{\hat{x}}(k)$, $\dot{\hat{y}}(k)$, $\dot{\hat{z}}(k)$ representing the target's position and velocity estimates, $\hat{b}(k)$ representing the radar measurements related uncertain scale coefficients estimates,

$$\Phi(k) = \begin{bmatrix} \mathbb{I}_{3\times3} & \mathbb{O}_{3\times3} \\ \mathbb{O}_{3\times3} & \delta t\mathbb{I}_{3\times3} \end{bmatrix},\ G(k) = \begin{bmatrix} 1/2\delta t^2\mathbb{I}_{3\times3} \\ \delta t\mathbb{I}_{3\times3} \end{bmatrix}$$

are the state transition and the influence matrices, $P(k)$ is the estimation error covariance matrix, Γ is a diagonal matrix of the process noise $n_x(k)\ \ n_y(k)\ \ n_z(k)\ \ n_b(k)$ variances σ_x^2, σ_y^2, σ_z^2, σ_b^2 respectively, $W(k)$ is the Kalman gain, $\boldsymbol{h}(k)$, $\hat{\boldsymbol{h}}(k|k-1)$ are respectively the available at time k measurement and measurement estimate computed at $\boldsymbol{s}(k|k-1))$, and $M(k|k-1)$ is the measurement Jacobean matrix evaluated at $\boldsymbol{s}(k|k-1))$. The detailed description of the EKF setup and implementation are given in the Ref. [13].

VI. Simulation Results

We evaluate the approach in desktop simulations using synthetic data generated for a target UAV of a size of DJI M600 flying along a planned trajectory for the upcoming flight test at NASA Ames Research Center's DART site. The distributed sensor infrastructure includes three identical ground-based radars and four identical ground based cameras (visual sensors) placed at four observation stations, which are designated by yellow circles on the site map displayed in the Figure 3. The communication towers and computing centers are respectively designated by gray and green circles on the same figure.

The target's motion was generated in Reflection simulation environment and recorded at 100 Hz. The recorded flight data are used to generate sensors readings using in-house developed radar and camera models with selected parameters and noise characteristics presented in Table 1.

For this simulation study, we assume that the radars are stationary, but the cameras are placed on the mobile platforms and can be flown at any time. The sensors initial locations, directions and fields of views (FOV) are displayed in Fig. 4. It is also assumed that the cameras provide target's information at a rate of 30 Hz in the form of compressed frames of size 0.4 $Mbts$ and the radars provide information at a rate of 10 Hz in the form of azimuth, elevation and range measurements of size 20 $Kbts$. All sensors transmit the measurements as soon as they become available over the witless links to the closest communication towers denoted as T_1, T_2, T_3, which wirelessly communicate among themselves. Communication towers are wired connected to computing centers C_1, C_2, C_3. According to the sensing, communication and computing infrastructure distribution presented in Fig. 3, radar R_1 and visual sensors V_1, V_4

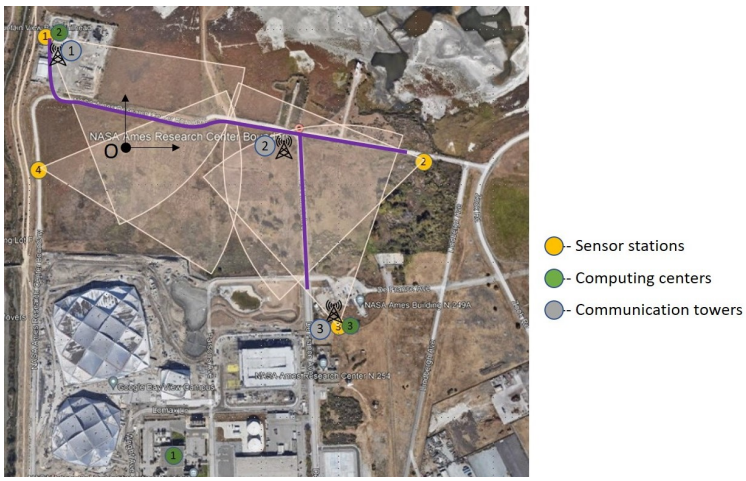

Fig. 3 Target's flight path, Sensor stations, Computing canters and Communication towers.

Camera parameters						
$Resolution$	$Size(mm)$	$H-FOV$	$F-length$	$Visible\ size$	σ_{p_x}	σ_{p_y}
[3600, 2700]	[14.4, 10.8]	$[-45°, 45°]$	7.2 mm	7 $pixel$	0.83387	0.4690
Radar parameters						
$H-FOV$	$V-FOV$	$Range(m)$	σ_ϕ	σ_θ	$\sigma_r(m)$	b
$[-60°, 60°]$	$[-40°, 40°]$	[20, 2000]	1°	3°	3.25	0.05

Table 1 Sensors Simulation Parameters.

initially communicate with tower T_1, and radars R_2, R_3 and visual sensors V_2, V_3 initially communicate with tower T_3. Computing centers C_1, C_3 are connected to tower T_3, and computing center C_2 is connected to communication towers T_1. It follows from the presented simulation scenario setup and selected parameters that no visual sensor can cover the gray shaded are in the figure 4.

Two computing centers C_2, C_3 are laptops at sensor stations S_1, S_3, and C_1 is using NASA super-computing center resources. The communication and computing parameters used for this simulation study are presented in the Table 2.

Communication parameters						
ω	c	w^s	w^t	B_{sys}	σ_a	g_0
200 $Mbts$	299.79e6 m/s	0.2 W	0.9 W	5MHz	2.83$e-07$	5.43$e-04$
Computation parameters						
λ_T	λ_{C_1}	λ_{C_2}, λ_{C_3}	α_T	α_{C_1}	α_{C_2}	α_{C_3}
2.2e7	2.2e9	2.2e9	32	32×4	32×4	32×1048

Table 2 Communication and computation Simulation Parameters.

The maximum distance for a reliable wireless transmission was set to 500 m for this simulation, which results in using tower T_2 for transmitting data between the towers T_1 and T_3. For the initial infrastructure distribution, the optimal data migration algorithm selects the computing center C_1 for the target tracking algorithm execution, with the initial information delays presented in Table 3 as number of time steps. It can be observed that the radar measurements are received by the tracking algorithm practically without any delay because of the transmitted package small size. The zero delay in V_3 measurement is attributed to the close proximity of the communication tower and the computing center. The delays in other visual sensor measurements arrivals are attributed to relatively large package size and the distances

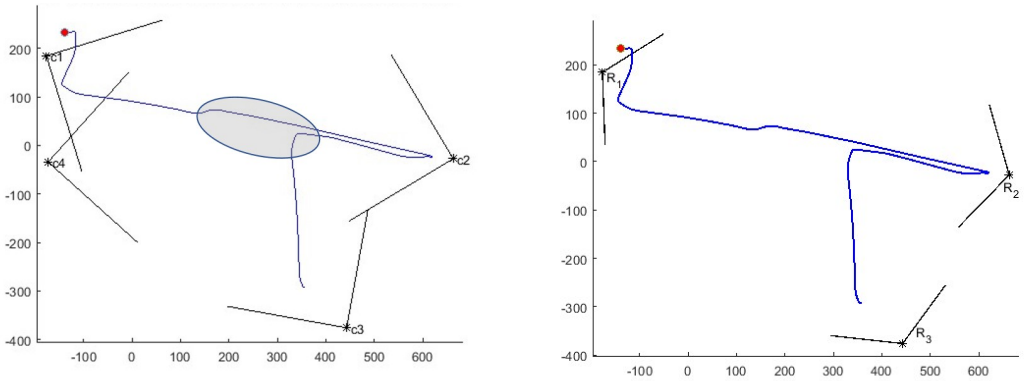

(a) cameras **(b) radars**

Fig. 4 Target's flight path, sensors locations, directions and fields of views

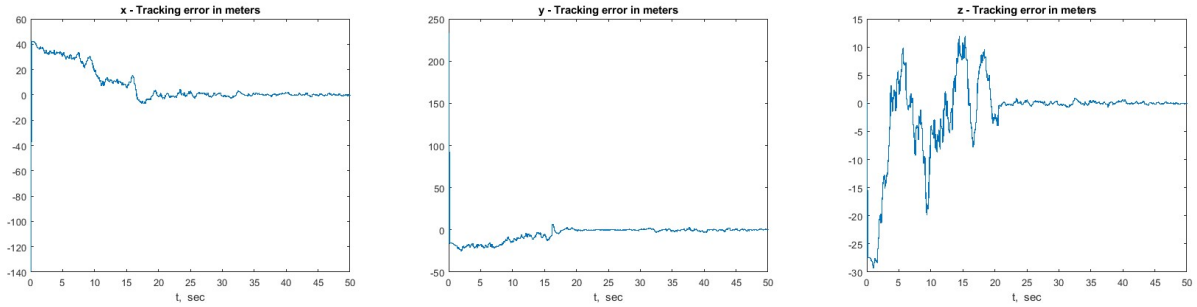

(a) x-error **(b) y-error** **(c) z-error**

Fig. 5 Target tracking errors for initial 50 seconds.

to travel to c_1 .

V_1	V_2	V_3	V_4	R_1	R_2	R_3
2	1	0	3	0	0	0

Table 3 Sensors data latency in time steps.

We initialize the filter's position state at the first radar measurement translated into the inertial frame as it becomes available. The velocity state and the unknown constant estimate, which is the same for all radars, are initialized at zero. The tracking error covariance matrix is initialized using the process noise variances and is set to $\Gamma = diag\left(50^2,\ 50^2,\ 50^2,\ 0.05^2\right)$.

For the fist 50 *sec* we implement EKF with stationary sensors until the initialization error effects die out and EKF converges. The corresponding tracking errors are presented in the Fig. 5.

At this stage, the target's position and direction of motion estimates are available for optimal configuration computation. We only move visual sensors V_1 and V_4, since the target is moving away from them. For this computation we set $\rho^{\min} = 40\ m$, $\rho^{\max} = 80\ m$, and $\rho = 22\ m$ for both sensors. The sensor carrying aircraft size is set to $r = 1.2\ m$ (known size), and the radius of target's uncertainty ball is set to $r_a = 5\ m$ (conservative estimate). Visual sensors V_1 and V_4 start the motion at 50 *sec*, and track the optimal configuration following at the same time target's estimated state until the minimum distance between mobile and stationary sensors becomes less than 400 m, after which they just hover at the same position and rotate the fields of view to keep the target as close to the focal axes as possible. Fig. 6 displays the mobile sensors and target's coordinates time histories.

To better understand the benefits of sensor mobility, we ran simulations for the ideal case setting all delays to zero

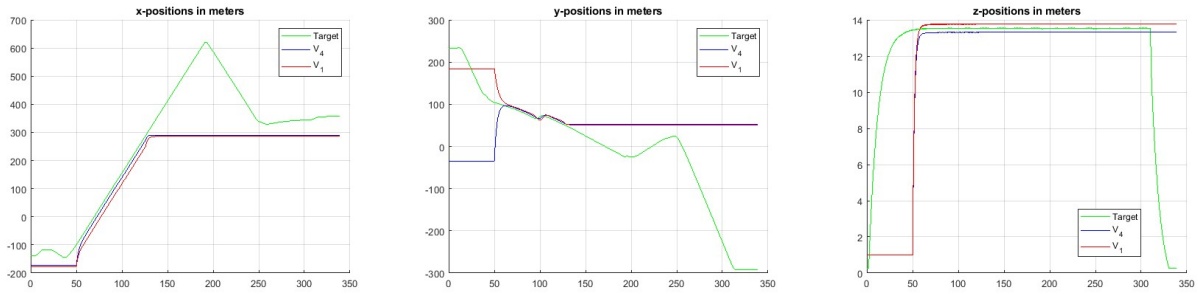

(a) x-error **(b) y-error** **(c) z-error**

Fig. 6 Mobile sensors coordinates time histories in meters

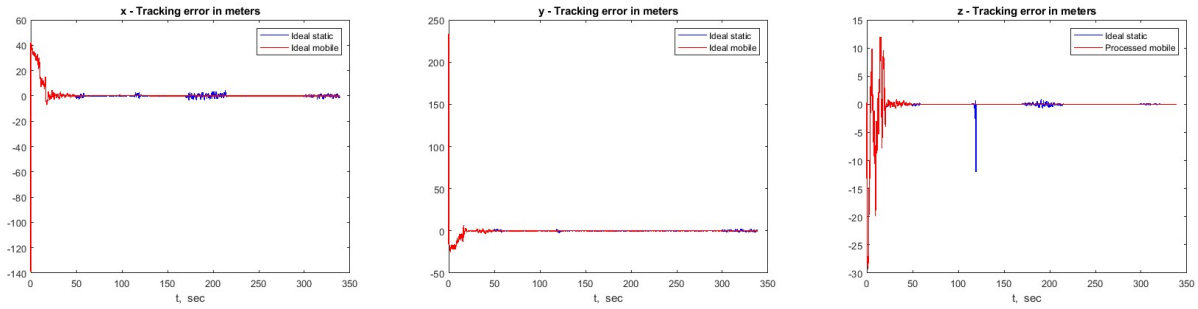

(a) x-error **(b) y-error** **(c) z-error**

Fig. 7 Tracking errors for stationary and mobile sensors in the ideal case, in meters.

for the stationary and mobile visual sensor cases. Fig. 7 displays the corresponding tracking errors. It can be observed that the sensors mobility improves the tracking as the sensors move closer to the target, especially in the gray shaded area mentioned earlier, where the stationary visual sensors do not have coverage, and in the final phase of landing, because the mobile sensors are able to see the target.

The corresponding root-mean-square values of the tracking errors and the trace of estimation covariance matrix are presented in Table 4

$Tracking\ case$	$RMS(e_x)$	$RMS(e_y)$	$RMS(e_z)$	$RMS(P_{tr})$
$Ideal\ stationary$	6.1927	5.0951	2.7388	40.121
$Ideal\ mobile$	6.1655	5.0837	2.7095	38.368

Table 4 Root-mean-square values of the tracking errors and of the trace of covariance matrix in ideal case.

We run optimal migration algorithm with an interval of $1sec$. As the sensors move closer to tower T_2, the communication delays for both of them reduce to one time step, but the EKF execution location remains C_1 because of the available high computing power. The detailed results of the EKF implementation with sensor mobility and periodically computed communication delays are presented in Figs. 8, 9, and 10 for the target's flight take-off, cruising and landing stages.

It can be observed large initial tracking errors in Fig. 8 because of the inaccurate initialization, which however get quickly decreased. As it can be inferred from figure 4 only radars provide observations at this stage, hence there is a comparably large tracking error in z-direction, because radars have noisier elevation measurements.

Figure 9 displays the tracking errors for the cruising phase, where the bursting at about 15 sec can be attributed to target's turning maneuver. The remaining large errors are drastically decreased after two visual sensors move closer to the target starting from 50 sec.

Tracking of the target in landing is displayed in Figure 10. The errors are very small, because the target is in the

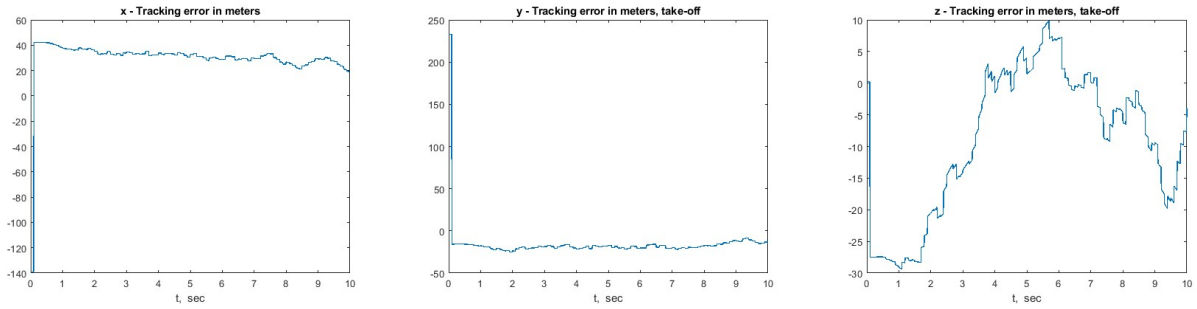

(a) x-error **(b) y-error** **(c) z-error**

Fig. 8 Target tracking errors during takeoff in meters.

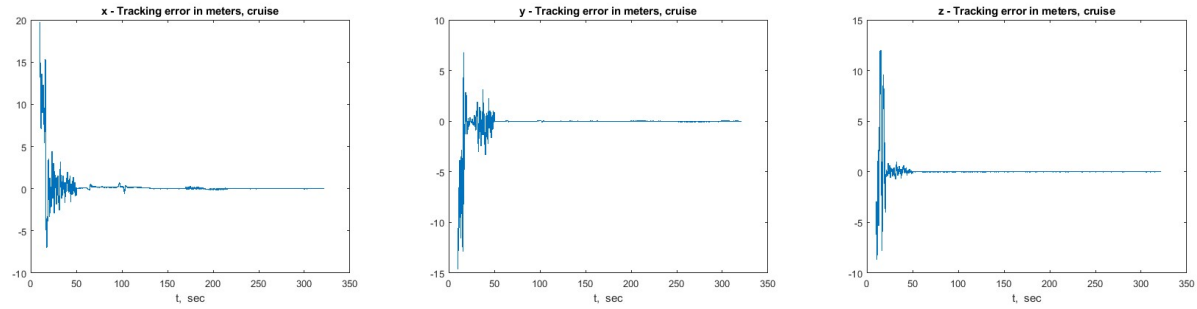

(a) x-error **(b) y-error** **(c) z-error**

Fig. 9 Target tracking errors during cruising in meters.

center of cameras V_1 and V_4 field of view during this stage.

The corresponding root-mean-square values are presented in Table 5. As we expected, initial large errors are decreased as the simulation progresses. However, somewhat large values in the cruise stage can be attributed to estimation errors in target's state, which is used to compute the sensors motion. In the last stage, these values are very small because the cameras V_1 and V_4 provide information from the stationary position, while keeping the target close to the center of FOV.

Fig. 11 displays convergence of the estimate of unknown constant b in radar measurements to the true value, which was set to $b = 0.05$. A good convergence can be observed after the initialization error dies out. It can be attributed to the fact that b is in the radar measurements, which practically have no delays.

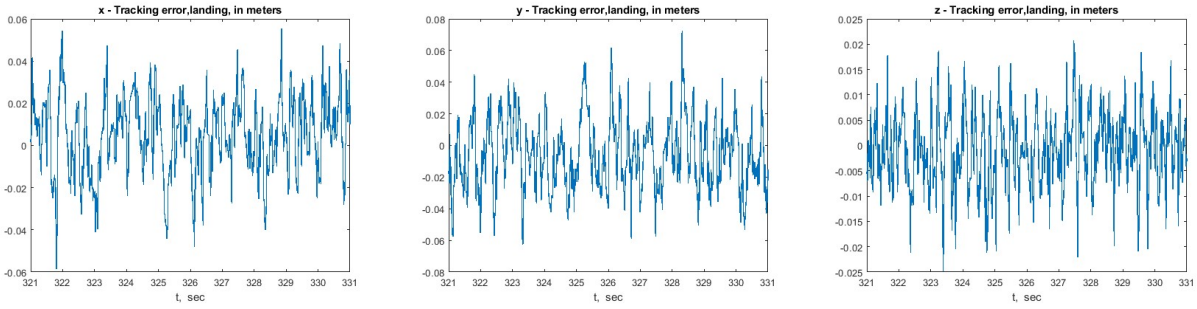

(a) x-error **(b) y-error** **(c) z-error**

Fig. 10 Target tracking errors during landing

$Time\ inreval$	$RMS(e_x)$	$RMS(e_y)$	$RMS(e_z)$	$RMS(P_{tr})$
$0 < t \leq 10$	34.623	28.702	14.579	164.98
$10 < t \leq 321$	1.6923	1.2889	1.0773	26.973
$321 < t \leq 331$	0.0193	0.0232	0.0075	4.8432

Table 5 Error root-mean-square values for takeoff, cruise and landing stages.

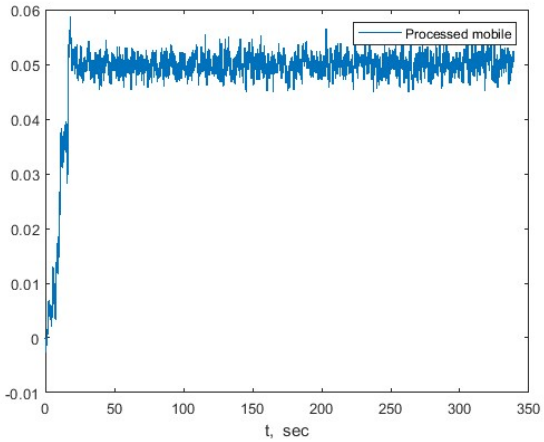

Fig. 11 Estimate of unknown constant b

VII. Conclusion

We have presented a flying target tracking approach fusing information from distributed stationary and mobile sensor network, which is transmitted through a wireless/wired communication network to a distributed computing infrastructure. To obtain high quality measurements, sensors flight platforms' positions and orientations are optimized with respect to available target's position and velocity estimates, and a formation control strategy is applied to derive desired trajectories for the flight platforms. As sensors move, the communication network topology switching is determined using the worst-case approach to handle uncertainties in the target's and sensors' positions. The optimal data migration algorithm is periodically applied to determine communication delays for each sensor and the tracking algorithm execution location, which uses the Extended Kalman Filter framework based on the adaptive information fusion from multi-modal mobile and stationary sensors. The approach is validated in a desktop simulation environment using synthetic sensor data generated for a simulated target's flight. It is concluded that the sensors mobility improves the tracking accuracy as a result of better sensor positioning and decreased communication delays.

Future research will include mobile antennas and computing centers, which will bring more complexity in the network design from the perspective of optimal wireless communication coverage, data migration and minimum latency computation, but will improve the tracking accuracy.

Acknowledgment

This work was performed under the NASA Aeronautics Research Mission Directorate (ARMD), Transformational Tools and Technologies (TTT) Project's Autonomous Systems activity.

References

[1] C. A. Ippolito, K. E. Hashemi, E. Kawamura, G. E. Gorospe, W. Holforty, K. Kannan, V. Stepanyan, T. Lombaerts, N. Brown, A. M. Jaffe and C. Dolph. Distributed Sensing and Advanced Perception Technologies to Enable Advanced Air Mobility. *AIAA SciTech Forum, Jan 2023. https://doi.org/10.2514/6.2023-0894*.

[2] C. A. Ippolito, E. Kawamura, G. E. Gorospe, W. Holforty, K. Kannan, V. Stepanyan, T. Lombaerts, N. Brown, A. M. Jaffe

and C. Dolph. A Structurally-Adaptive Framework for Distributed Airborne Sensing over Real-time Collaborative Information Sharing Networks. *AIAA SciTech Forum, Jan 2023. https://doi.org/10.2514/6.2023-2680*.

[3] F. E. Daum and R. J. Fitzgerald. Decoupled Kalman Filters for Phased Array Radar Tracking. *IEEE Transactions on Automatic Control, Vol. Ac-28, No. 3, March 1983* , page 269-283, doi: 10.1117/12.492752

[4] L. Mo, X. Song, Y. Zhou, Z. Sun, and Y. Bar-Shalom. Unbiased converted measurements for tracking. *IEEE Transactions on Aerospace and Electronic Systems, Vol. 34, No. 3, 1998*, page 1023–1027

[5] Y. Bar-Shalom, X. R. Li, and T. Kirubarajan. Estimation with Applications to Tracking and Navigation: Theory, Algorithms, and Software. *New York: Wiley, 2001*

[6] X. R. Li and V. P. Jilkov. Survey of Maneuvering Target Tracking. Part I: Dynamic Models. *IEEE Transactions on Aerospace and Electronic Systems, Vol. 50, No. 12, April 2014*, page 1431-1444

[7] Z. Duan, C. Han, and X. R. Li. Comments on unbiased converted measurements for tracking. *IEEE Transactions on Aerospace and Electronic Systems, Vol. 40, No. 4, 2004*, page 1374–1377

[8] A. N. Bishop, P. N. Pathirana, and A. V. Savkin. Radar Target Tracking via Robust Linear Filtering. *IEEE Signal Processing Letters, Vol. 14, No. 12, December 2007*, page 1028-1031, doi: 10.1109/LSP.2007.907993

[9] S. Bordonaro, P. Willett, and Y. Bar-Shalom. Decorrelated, Unbiased Converted Measurement Kalman Filter. *IEEE Transactions on Aerospace and Electronic Systems, Vol. 39, No. 4, October 2003*, page 1333-1364

[10] D. Crouse. Basic tracking using nonlinear continuous-time dynamic models. *IEEE Aerospace and Electronic Systems Magazine, Vol. 30, No. 2, 2015*, page 4-41

[11] C. Dolph, T. Lombaerts, E.'Kawamura, C. A. Ippolito, V. Stepanyan, K. Iftekharuddin, G. Szatkowski, R. McSwain, C. Morris, M. R. Malekpour and C. Minwalla Ground to Air Testing of a Fused Optical-Radar Aircraft Detection and Tracking System. *AIAA SciTech Forum, Jan 2022. https://doi.org/10.2514/6.2022-0498*.

[12] T. Lombaerts, K. Kannan, E. Kawamura, C. Dolph, V. Stepanyan, G. Gorospe and C. A. Ippolito. Distributed Ground Sensor Fusion Based Object Tracking for Autonomous Advanced Air Mobility Operations. *AIAA SciTech Forum, Jan 2023. https://doi.org/10.2514/6.2023-0896*.

[13] V. Stepanyan, K. Kannan, E. Kawamura, T., Lombaerts, and C. Ippolito. Target Tracking with Distributed Sensing and Optimal Data Migration. *AIAA SciTech Forum, Jan 2023. https://doi.org/10.2514/6.2023-2194*.

[14] L. Dihel, C. Dolph, H. T. Holbrook and S. Roy. Classifying Aircraft using Velocity Data with Support Vector Machines and Likelihood Ratio Tests. *AIAA SciTech Forum, Jan 2023. https://doi.org/10.2514/6.2023-0898*.

[15] E. J. Rodríguez-Seda, J. J. Troy, C. A. Erignac, P. Murray and D. M. Stipanovic Bilateral Teleoperation of Multiple Mobile Agents: Coordinated Motion and Collision Avoidance. *IEEE Transactions on Control Systems Technology, Vol 18, No. 4, 2010, pp. 984-992. https://doi.org10.1109/TCST.2009.2030176*.

[16] J. Wang and M. Xin. Integrated Optimal Formation Control of Multiple Unmanned Aerial Vehicles. *IEEE Transactions on Control Systems Technology, Vol 21, No. 5, 2013, pp. 1731-1744. https://doi.org10.1109/TCST.2012.2218815*.

[17] K.-K. Oa, M.-C. Park and H.-S. Ahn. A Survey of Multi-Agent Formation Control. *AIAA SciTech Forum, Jan 2022. https://doi.org/10.1016/j.automatica.2014.10.022*.

[18] J. Sun, J. Tang and S. Lao. Collision Avoidance for Cooperative UAVs With Optimized Artificial Potential Field Algorithm. *IEEE Access, Vol.5, September 2017, pp. 18382-18390. DOI: 10.1109/ACCESS.2017.2746752*.

[19] H. Kang, W. Wang, C. Yang and . Li. Leader-Following Formation Control and Collision Avoidance of Second-Order Multi-Agent Systems With Time Delay. *IEEE Access, Vol.8, August 14, 2020, pp. 142571-142580. DOI: 10.1109/ACCESS.2020.3012992*.

[20] A. Marchidan and E. Bakolas. Collision Avoidance for an Unmanned Aerial Vehicle in the Presence of Static and Moving Obstacles. *Journal of Guidance, Control, and Dynamics, Vol. 43, No. 1, January 2020, pp. 96-110. DOI: 10.2514/1.G004446*.

[21] L. Dai, B. Wang, Y. Yuan, S. Han, C. -L. I, and Z. Wang. Non-orthogonal multiple access for 5G: Solutions, challenges, opportunities, and future research trends. *IEEE Commun. Mag., vol. 53, no. 9, pp. 74–81, Sep. 2015*.

[22] S. Hu and G. Li. Dynamic Request Scheduling Optimization in Mobile Edge Computing for IoT Applications. *IEEE Internet of Things Journal, Vol. 7, No. 2, February 2020*.

[23] V. Stepanyan, S. Schuet and K. S. Krishnakumar. An Approach to Reasoning Service Migration in Data and Reasoning Fabric (DRF) Implementation. *AIAA SciTech Forum, Jan 2022. https://doi.org/10.2514/6.2022-0787*.